7816–7827 *Nucleic Acids Research, 2011, Vol. 39, No. 17* *Published online 7 June 2011*
doi:10.1093/nar/gkr419

The structural basis for partitioning of the XRCC1/DNA ligase III-α BRCT-mediated dimer complexes

Matthew J. Cuneo, Scott A. Gabel, Joseph M. Krahn, Melissa A. Ricker and Robert E. London*

Laboratory of Structural Biology, National Institute of Environmental Health Sciences, NIH, DHHS, Research Triangle Park, NC

Received March 28, 2011; Revised May 9, 2011; Accepted May 10, 2011

ABSTRACT

The ultimate step common to almost all DNA repair pathways is the ligation of the nicked intermediate to form contiguous double-stranded DNA. In the mammalian nucleotide and base excision repair pathways, the ligation step is carried out by ligase III-α. For efficient ligation, ligase III-α is constitutively bound to the scaffolding protein XRCC1 through interactions between the C-terminal BRCT domains of each protein. Although structural data for the individual domains has been available, no structure of the complex has been determined and several alternative proposals for this interaction have been advanced. Interpretation of the models is complicated by the formation of homodimers that, depending on the model, may either contribute to, or compete with heterodimer formation. We report here the structures of both homodimer complexes as well as the heterodimer complex. Structural characterization of the heterodimer formed from a longer XRCC1 BRCT domain construct, including residues comprising the interdomain linker region, revealed an expanded heterodimer interface with the ligase III-α BRCT domain. This enhanced linker-mediated binding interface plays a significant role in the determination of heterodimer/homodimer selectivity. These data provide fundamental insights into the structural basis of BRCT-mediated dimerization, and resolve questions related to the organization of this important repair complex.

INTRODUCTION

The repair of damaged DNA requires the coordinated action of multiple enzymes that interpret the damage, excise the damaged components and re-synthesize the DNA. X-ray cross complementing group 1 protein (XRCC1) is a scaffold protein that plays a central role in the organization of the base excision repair (BER) and single-strand break (SSB) repair pathways by interacting with and mediating interactions between the repair proteins (1). Of the multiple binding partners that have been identified (2–5), only one, DNA ligase III-α (L3α), forms a constitutive XRCC1 complex (6). Efficient DNA nick ligation involves the participation of the XRCC1/L3α complex that is mediated through the interaction of the C-terminal BRCT domains of both proteins (7). This interaction is required to maintain normal levels of DNA ligase activity and DNA ligation is defective in the absence of an XRCC1/L3α complex (6). In addition to the more extensively studied roles of the XRCC1/L3α in the SSB and BER pathways, recent studies indicate that the XRCC1/L3α complex is also utilized for the final ligation step in the nucleotide excision repair (NER) pathway in both dividing and non-dividing cells (8). There is also evidence that the XRCC1/L3α complex participates as a backup alternative in the non-homologous end-joining pathway (9).

Although structural data has been available for the C-terminal L3α BRCT (L3BRCT) and XRCC1 BRCT (X1BRCTb) domains (10,11), the nature of the complex that mediates the interaction of X1BRCTb and L3BRCT has been unclear, and alternative structural proposals involving different interfaces and stoichiometries have been advanced (7,12,13). Dulic *et al.* (13) modeled the

*To whom correspondence should be addressed. Tel: 919 541 4879; Fax: +919 541 5707; Email: london@niehs.nih.gov

The authors wish it to be known that, in their opinion, the first two authors should be regarded as joint First Authors.

L3BRCT domain based on sequence homology with X1BRCTb and further proposed a heterodimeric X1BRCTb/L3BRCT structure analogous to the X1BRCTb homodimer observed in the crystal. In general, it is unclear why the repair proteins would utilize a common interface allowing both homo- and heterodimer formation, resulting in competitive dimerization interactions. Alternatively, Beernink *et al.* (12) proposed that since both X1BRCTb and L3BRCT form stable homodimers, the biologically active unit involves a BRCT tetramer formed by the association of the two BRCT homodimers. Based on these studies, they determined that the association rate of the heterodimer was too fast to account for displacement of the homodimers (12). According to this model, the biologically active unit involves two copies of XRCC1 and L3α forming the biochemically observed tetrameric quaternary complex. Alternatively, Taylor *et al.* (7) have identified a different X1BRCTb/L3BRCT dimerization interface, centered around the α2–α3 loop residues 573–592 in X1BRCTb. These alternative models have important implications for understanding the function of the XRCC1/L3α repair complex and for the interpretation of XRCC1 nucleotide polymorphism data that is becoming available (14,15).

To resolve competing models and to further understand the basis of this BRCT heterodimerization, we have obtained structural and biochemical data on both mouse X1BRCTb and human L3BRCT homodimers, as well as on the X1BRCTb/L3BRCT heterodimer. Although the L3BRCT homodimer interface is similar to that observed for X1BRCTb, several important side-chain mediated interactions are not conserved between the two interfaces. These differences are postulated to result in a weaker homodimerization binding constant for L3BRCT relative to X1BRCTb. More significantly, analysis of the structure of the X1BRCTb/L3BRCT heterodimer suggested that additional heterodimer stabilization results from the interaction of residues in the N-terminal linker region immediately preceding the X1BRCTb domain, with a hydrophobic region on the L3BRCT domain. Compelling support for the importance of these interactions has been derived from crystallographic and biochemical studies. These results provide fundamental insights not only regarding the organization of this important DNA repair complex, but additionally reveal previously unknown mechanisms by which protein homo- and heterodimeric interactions among BRCT containing proteins can be modulated.

MATERIALS AND METHODS

Cloning overexpression and purification

The mouse X1BRCTb domain (residues 535–631) and the human L3BRCT domain (residues 836–921) genes were synthesized and cloned into a pUC18 vector by Genscript. The human ligase III-α gene, with an N-terminal hexahistidine tag followed by a TEV protease cleavage site, was subcloned into pETDuet-1 Vector. The X1BRCTb gene, followed by a C-terminal hexahistidine tag was subcloned into a pET21a vector. For co-expression with L3BRCT, the X1BRCTb construct, lacking any purification tag, was subcloned into a pCOLADuet-1 vector. For crystallization of the heteroprotein complex, an X1BRCTb Y574R mutant was also constructed in a pCOLADuet-1 vector. The same construct was used to build the X1BRCTb extended, however, the amino acid sequence QEPPDLPV, corresponding to the human XRCC1, was added to the N-terminus of the protein using PCR. For analytical gel filtration, an X1BRCTb L596R mutant was constructed. For SAXS analysis, a double mutant (Y574R/L596R) X1BRCTb was utilized.

Plasmids were transformed into BL21-DE3-RIL cells and grown in auto-induction media or on LB media supplemented with the appropriate antibiotics. In either case, at an OD600 of 0.5–1.0, the cultures were cooled to 20°C and allowed to auto-induce, or were induced with 1 mM IPTG, for a total of 18 additional hours. The cells were harvested by centrifugation (5000 *g* for 10 min), resuspended in 20 mM imidazole, 20 mM Tris, 500 mM NaCl (pH 7.5) and lysed by sonication. A cleared lysate was prepared by centrifugation. Proteins were purified by immobilized metal affinity chromatography. A step gradient of 20, 75 and 400 mM imidazole (with 20 mM Tris pH 7.5 and 500 mM NaCl) was employed. The protein eluted in the 400 mM aliquot. For TEV protease digestion, proteins were dialyzed into phosphate-buffered saline (PBS) and allowed to digest overnight at 4°C. Proteins were further purified on a Superdex 26/60 S75 (Amersham) gel filtration column. For analytical gel-filtration, 80 µl of protein was loaded onto a Superdex S75 GL column that was pre-equilibrated with 20 mM Tris–HCl (pH 7.8) and either 150 mM NaCl or 1 M NaCl. A flow rate of 0.5 ml/min was used.

Heteroprotein complexes were co-expressed and co-purified as above and in all cases produced using his-tagged L3BRCT co-expressed with X1BRCTb lacking any tags. Selenomethionine labeled L3BRCT was produced and purified as above with the exception that B834 methionine auxotrophic cells and minimal media supplemented with 80 mg/ml of selenomethionine was used.

SAXS data acquisition and processing

SAXS data were collected at room temperature on the X9 beam line at the National Synchrotron Light Source (Brookhaven National Laboratory). The wavelength of the beam was 0.92 Å and the sample to detector distance was two meters. The heterodimeric double mutant (X1BRCTb (Y574R and L596R /wt-L3BRCT) (2.0–8.0 mg/ml) collected from a gel filtration column were concentrated and dialyzed into a 20 mM Na Phosphate, 1.0 mM TCEP and 140 mM NaCl pH 7.5 buffer for SAXS analysis; SAXS data was collected on three dilutions of protein (Supplementary Table S4). Scattering data were circularly averaged and scaled to obtain a relative scattering intensity (I) as a function of momentum transfer vector, q ($q = [4\pi sin\theta/\lambda)$, after subtraction of buffer scattering contributions.

SAXS data analysis and model construction

All scattering data were analyzed using the Primus software package (16); the GNOM45 software package (17) was used for all $P(r)$ and I_0 analyzes. The radius of gyration, R_g and forward scattering, I_0, were calculated from the second moment and the start of $P(r)$, respectively. R_g is the root mean square of all elemental volumes from the center-of-mass of the particle, weighted by their scattering densities and I_0 is directly proportional to the molar particle concentration multiplied by the square of the scattering particle molecular weight for particles with the same mean scattering density. Guinier plots were linear over a q-range of 0.017–0.071 Å.

Three-dimensional shape of the heterodimer was constructed from the SAXS data using the GASBOR22IQW program (q-range input for analysis was from 0.017 to 0.3 Å) (18), by calculating the distribution of linearly connected 1.9 Å spheres that best fit the scattering data. Each calculation was repeated at least five times with different random starting points for the Monte Carlo optimization algorithm; no predefined shape or symmetry constraints were used. From these runs, the predicted structure with the lowest deviation of the calculated scattering profile from experimental data was used for interpretation. To compare the SAXS-based models with the atomic structures, the SUPCOMB13 (19) program was used.

Circular dichroism temperature melts

Circular dichroism (CD) measurements were carried out on a Jasco spectrophotometer. Thermal denaturations were determined by measuring the CD signal at 225 nm (1 cm path length) as a function of temperature, using 2.5 μM protein (10 mM Tris–HCl pH 7.8, 20 mM NaCl, 0.5 mM TCEP). Data were fit to a two-state model to determine the $^{app}T_m$ values (20,21).

Crystallization and data collection

All crystals were grown using hanging drop vapor diffusion, mixing 2 μl of the precipitant solution with 2 μl of the protein solution and equilibrating over 900 μl of precipitant solution. The L3BRCT domain (12 mg/ml dialyzed into 10 mM Tris, 50 mM NaCl) was crystallized using 25–35% polyethylene glycol 3350, 0.1 M Bis–Tris, pH 6.5, 0.25 M ammonium acetate as a precipitant and frozen in 35% (w/v) polyethylene glycol 3350 for cryoprotection. Purified X1BRCTb (12 mg/ml dialyzed into 10 mM Tris, 50 mM NaCl) was crystallized using 0.5–0.7 M Na Formate, pH 7.2–7.5, 0.2 M Na HEPES as a precipitant and frozen in 20% (w/v) ethylene glycol for cryoprotection. The X1BRCTb(Y39R)/L3BRCT complex (21 mg/ml dialyzed into 10 mM Tris, 50 mM NaCl and 1 mM TCEP) was crystallized using 30% PEG 4000, pH 8.5, 0.1 M Tris and 0.2 M $MgCl_2$ as a precipitant and cryoprotectant. Crystals of the X1BRCTb-extended/L3BRCT (21 mg/ml dialyzed into 10 mM Tris, 40 mM NaCl and 1 mM TCEP) were formed using 30% PEG 4000, pH 8.5, 0.1 M Tris and 0.2 M Na Acetate as a precipitant and cryoprotectant. X1BRCTb and L3BRCT data were collected at the SERCAT beamline at the Advanced Photon Source, Argonne National Laboratory at 100 K using a Mar345 CCD detector. The diffraction data were scaled and indexed using XDS (22). X1BRCTb(Y39R)/L3BRCT and X1BRCTb-extended/L3BRCT data were collected at 100 K on a Rigaku 007HF micromax X-ray generator with a Saturn92 CCD detector. The diffraction data were scaled and indexed using XDS (22) and HKL2000 (23), respectively.

Structure determination methods, model building and refinement

The crystal structure of human X1BRCTb (PDB code 1CDZ) was used to solve the structure of the mouse X1BRCTb to a resolution of 1.9 Å using the PHASER program (24). No Ramachandran outliers are present in the model and 99.5% are in the favored Ramachandran space.

The crystal structure of the mouse X1BRCTb was used to solve the structure of the human L3BRCT using the PHASER program (24). The solution was confirmed using the anomalous signals from the two selenium sites in the asymmetric unit. The L3BRCT structure was solved to a resolution of 1.65 Å. No Ramachandran outliers are present in the model and 98.1% are in the favored Ramachandran space.

The X1BRCTb(Y574R)/L3BRCT complex was solved to a resolution of 2.3 Å using the respective monomers from the X1BRCT band L3BRCT structures utilizing the PHASER program (24). One Ramachandran outlier is present in the model and 97.9% are in the favored Ramachandran space.

The X1BRCTb(Y574R)-extended/L3BRCT complex was solved to a resolution of 2.26 Å as above. No Ramachandran outliers are present in the model and 98.3% are in the favored Ramachandran space.

Manual model building was carried out in COOT and refined using REFMAC5 and PHENIX (25,26). PDB coordinates and structure factors have been deposited in the RCSB Protein Data Bank under the accession codes 3PC6, 3PC7, 3PC8, 3QVG for X1BRCTb, L3BRCT, X1BRCTb/L3BRCT complex and the X1BRCTb(Y574R)-extended/L3BRCT complex, respectively. Data collection, refinement and stereochemistry statistics are summarized in Table 1.

RESULTS

Crystal structure of homodimeric mouse X1BRCTb

Crystals of X1BRCTb were obtained from solutions containing both the X1BRCTb and the L3BRCT constructs, demonstrating the competitive stability of the X1BRCTb homodimer and its favorable crystallization. The X-ray crystal structure of mouse X1BRCTb was solved by molecular replacement, using the 3.2 Å resolution structure of human X1BRCT (PDB code 1CDZ) (11), to a resolution of 1.9 Å. The mouse X1BRCTb adopts the globular α/β-fold that is characteristic of BRCT domains and has a 0.5 Å RMSD of Cα atoms with the human X1BRCTb structure (Figure 1). The two monomers in the asymmetric unit correspond to the same homodimer interface

Table 1. Data collection and refinement statistics

	L3BRCT	X1BRCTb	X2BRCTb(Y39R)/ L3BRCT	extended-X2BRCTb(Y39R)/ L3BRCT
Resolution Range (Å)	50.0–1.65	50.0–1.90	35.0–2.31	35.0–2.26
Unique reflections	19 139	20 146	17 611	18 358
Redundancy	9.3 (8.8)	5.1 (3.5)	6.6 (5.4)	6.3 (3.3)
Mean $I/\sigma(I)$[a]	26.9 (4.8)	23.6 (4.8)	26.1 (6.4)	20.6 (4.9)
R_{merged} (%)[a]	6.9 (42.2)	6.2 (23.1)	5.3 (33.6)	7.1 (26.1)
Completeness (%)[a]	98.9 (100)	97.4 (82.8)	96.0 (83.2)	97.5 (80.4)
Unit cell				
Dimensions (Å)	a/b = 70.1 c = 62.3	a = 44.2 b = 56.9 c = 100.4	a = 66.3 b = 163.5 c = 36.7	a = 38.1 b = 61.5 c = 163.7
Angles (°)				
Space group	$P4_32_12$	$P2_12_12_1$	$P2_12_12$	$P2_12_12_1$
Non-hydrogen atoms in refinement				
Protein	1313	1761	2936	3060
Water	176	183	208	297
R_{cryst}/R_{free} (%)[b]	14.1/19.7	18.0/22.7	19.7/24.7	19.9/27.0
R.m.s.d. from ideal				
Bond lengths (Å)	0.008	0.006	0.004	0.003
Bond angles (°)	1.1	0.863	0.721	0.6
B-factors (Å^2)				
	Chain A = 26.9, Chain B = 28.8	Chain A = 27.1, Chain B = 26.1	Chain AC = 33.2, Chain BD = 38.4	Chain AB = 28.2, Chain CD = 31.2
Water	41.3	34.5	37.7	33.6

[a]Number in parentheses represent values in the highest resolution shell.
[b]R_{free} is the R_{factor} based on 5% of data excluded from refinement.

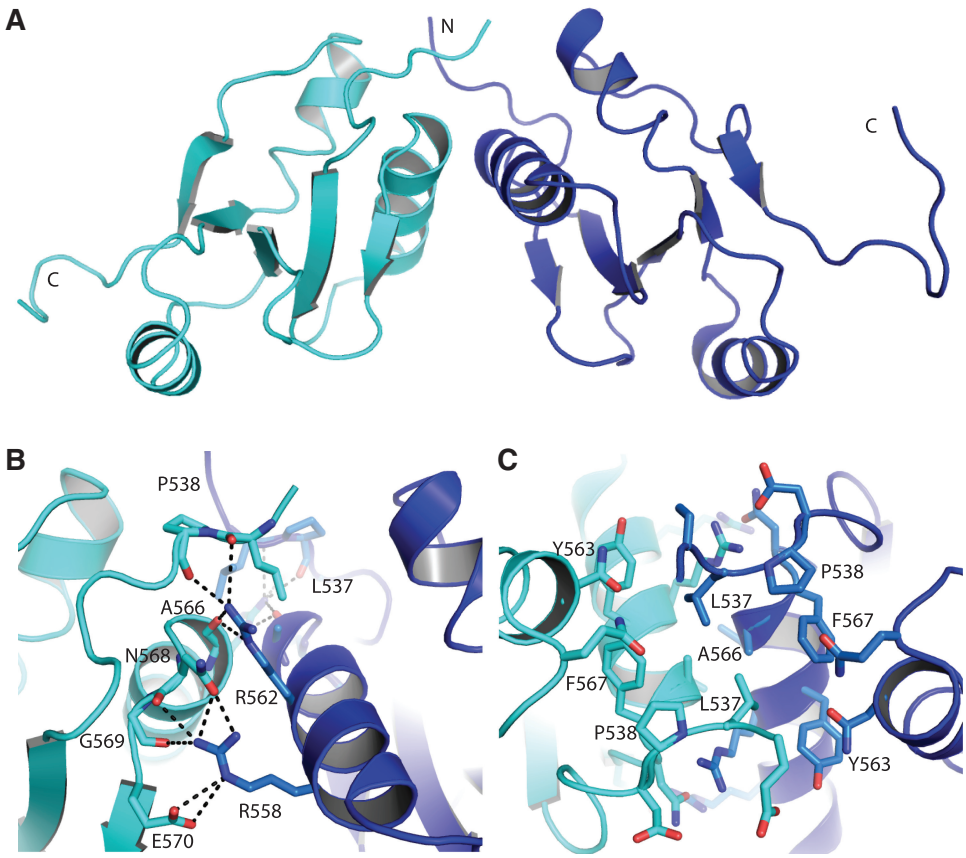

Figure 1. Structure of the X1BRCTb homodimer. (**A**) Ribbon diagram of the X1BRCTb homodimer. The monomers are colored in cyan and blue. (**B**) Close-up view of the hydrogen bonding network between X1BRCTb monomers. (**C**) Close-up view of the homodimer interface illustrating the hydrophobic contacts. Amino acid side-chains that are found to be part of the interface are represented as stick models. Labels are shown only for hydrophobic residues.

identified in the previous study (11). Additionally, even though the current X1BRCTb structure crystallized with a different unit cell and space group, a similar crystallographic symmetry mate is found interacting through the β4 and C-terminal region of each protein. Based on our gel-filtration data (below) of an L596R mutation at this interface, we demonstrate that this surface is important for tetramer formation.

Although consistent with the lower resolution structure, the higher resolution structure presented here allows for better modeling of the main- and side-chain atoms. A total of 19 hydrogen bonds are formed across the protein interface (Supplementary Table S1). The hydrogen-bonding pattern is not exactly symmetric across the homodimer. The side-chain of Asp539 is in an alternate rotamer in chain A whereas the rotamer in chain B allows formation of a hydrogen bond with the η hydrogen of Arg562. Additionally, electron density for the side-chain of Glu570 is not observed for chain B (Supplementary Table S1). The remainder of the interface consists of a network of non-polar amino acids in the core of the interface (Figure 1); all together polar and non-polar amino acids contribute a total of 1205 $Å^2$ of buried surface area to the interprotein interface.

Crystal structure of the homodimeric human L3BRCT

As with X1BRCTb, crystals of L3BRCT were obtained from solutions containing both the X1BRCTb and the L3BRCT constructs. The X-ray crystal structure of the human L3BRCT was solved by molecular replacement to a resolution of 1.65 Å, using a monomer from the mouse X1BRCTb structure (Figure 2). Two molecules are found in the asymmetric unit. Analysis of symmetry-related molecules reveals that two distinct crystallographic homodimers are formed with substantial interface contacts involving residues predicted to be at the interface by Dulic *et al.* (13) and consistent with the X1BRCTb homodimer interface (Figure 2). One of the L3BRCT homodimers adopts an orientation that is similar to that of the X1BRCTb homodimer (RMSD value of 1.8 Å for Cα atoms). The second L3BRCT homodimer is related to the first by a 13° difference in orientation of monomers across the homodimer interface, resulting in a more closed structure and altered protein interface (Figure 2).

In the homodimer that is structurally similar to X1BRCTb, a total of 16 hydrogen bonds are formed across the L3BRCT interface (Supplementary Table S2). Arg870, a structural analog of Arg562 in X1BRCTb, has seven potential partners within hydrogen bonding distance with the second monomer (Figure 2), interacting with the same conserved network of amino acids found in X1BRCTb. The remainder of the interface consists of a network of non-polar amino acids contributing a total of 1365 $Å^2$ of buried surface area (Figure 2).

In the second homodimer (Figure 2 and Supplementary Table S2), the hydrogen-bonding pattern of Arg870 is the same, however a hydrogen bond between Tyr871 and Leu847 is lost. The loss of this hydrogen bond is compensated by the formation of two additional hydrogen bonds pairing the side-chain of Arg869 with the main-chain of Leu879 and the side-chain of Asp878 (Figure 2). An additional hydrogen bond is also likely to be formed across the crystallographic 2-fold axis between the side-chain atoms of Gln881. The altered conformation of the two monomers also alters the non-polar surface of the interface. An additional hydrophobic region surrounding Gln881, contributes a total of ~50 $Å^2$ of buried surface area to the interface. The polar and non-polar amino acids of closed L3BRCT homodimer contribute a total of 1304 $Å^2$ of buried surface area in the interprotein interface, which is similar to the more open homodimer (Figure 2).

Crystal structure of the heterodimeric X1BRCTb/L3BRCT complex

As mentioned above, X1BRCTb and L3BRCT homodimer crystals were obtained in some of the studies designed to crystallize the X1BRCTb/L3BRCT heterodimer, demonstrating the competitive stability of the hetero- and homodimers. An alternate crystal form of the X1BRCTb homodimer revealed an additional symmetry-related molecule in whichTyr574 formed significant interactions with the X1BRCTb homodimer (Supplementary Figure S1). We hypothesized that a non-conservative substitution for Tyr574 would interfere with the observed interactions and facilitate alternate crystallization conditions that could include heterodimer structures. Consistent with this hypothesis, mutation of this residue to arginine resulted in crystallization of the desired X1BRCTb/L3BRCT heterodimer complex. The mutated Y574R residue is not involved in any of the crystallographic interfaces, although it does mediate lattice contacts. In support of the mutational strategy that we have adopted, the corresponding residue in the human XRCC1, Tyr576, exhibits an infrequent Y576S polymorphism, which appears not to influence either the stability or the function of the protein (15).

Consistent with the biochemically observed tetrameric quaternary structure, the four molecules found in the crystallographic asymmetric unit assemble into a homodimer of heterodimers (Figure 3). The interface of the two heterodimers involves only the two X1BRCTb domains. The two heterodimers adopt similar conformations with a Cα MSD of 0.7 Å; in the discussion below, the homodimer with the highest structural homology (0.2 Å RMSD for Cα atoms of heterodimer chains A/C) to the X1BRCTb is used. The X1BRCTb and L3BRCT interfaces involved in heterodimer formation are essentially identical with the interfaces used for homodimer formation. Similarly, the X1BRCTb homodimer interface is identical to the crystallographic protein interface that is observed in both the current and the previously determined X1BRCTb homodimers (11).

Numerous polar and non-polar interactions are present at the heterodimer interface with a total of ~1210 $Å^2$ of buried surface area forming the interprotein interface, while there are a total of 18 potential partners within hydrogen bonding distance with the second monomer. The residues involved in heterodimer hydrogen bonding

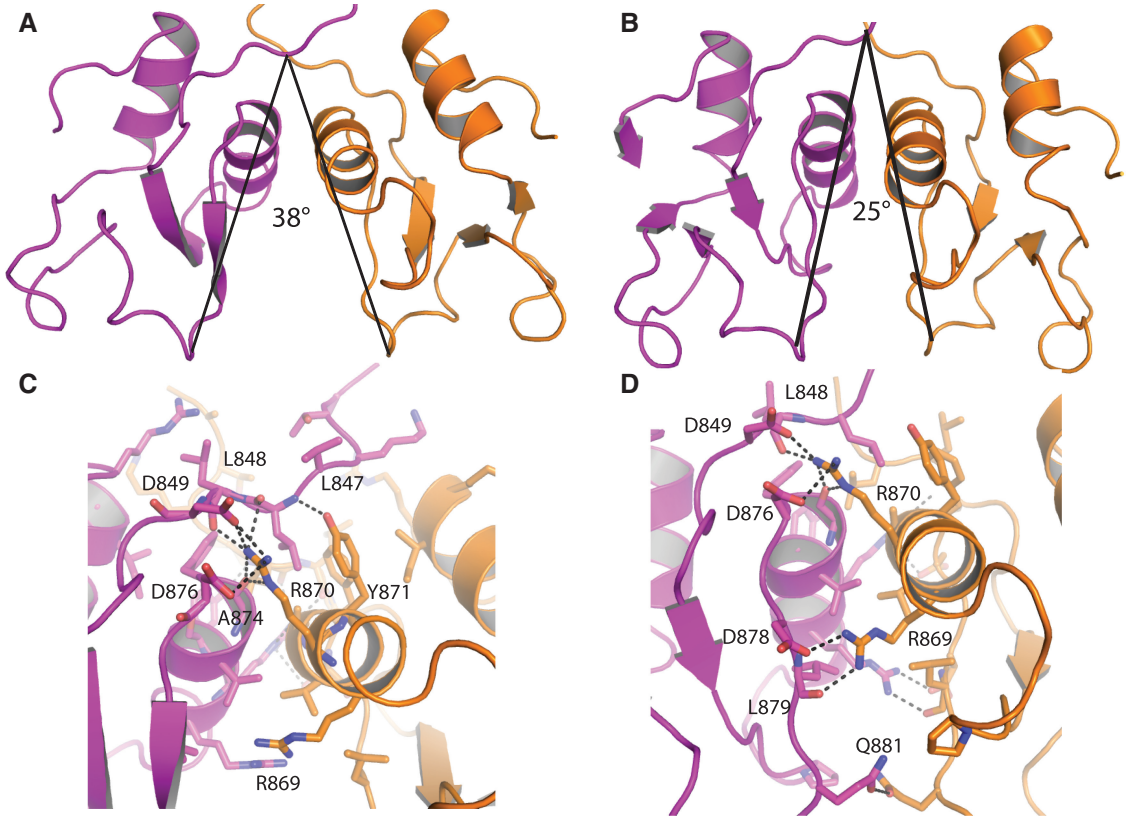

Figure 2. Structure of homodimeric L3BRCT. Two conformationally distinct homodimers were identified in the crystal structure and are shown in (**A**) and (**B**). The two structures differ by 13° in the relative orientation of the L3BRCT monomers. (**C**) Close-up view of the interface amino acids and hydrogen bonding network between the L3BRCTmonomers from the homodimer in (A). (**D**) Close-up view of the interface amino acids and hydrogen-bonding network between the L3BRCTmonomers from the homodimer in (B). Hydrogen bonds between monomers are represented as black dashed lines and residues involved in hydrogen bonds are labeled.

interactions are largely the same residues involved in the homodimer (Figure 3 and Supplementary Table S3). Arg558 and Arg562 from X1BRCTb each form four hydrogen bonds with L3BRCT. Arg869 from L3BRCT forms a hydrogen bond with the side-chain of Glu570 from X1BRCTb. Arg870 from L3BRCT forms four hydrogen bonds with X1BRCTb. The remaining interprotein hydrogen bonds are formed through the interaction of the hydroxyl of Tyr871 from L3BRCT with the main-chain carbonyl of Pro535 and the main-chain nitrogen of Leu537. We also note that although the heterodimer corresponds to the a complex of the mouse X1BRCTb with the human L3BRCT, none of the sequence differences involve interface residues.

The X1BRCTb homodimer interface in the tetramer corresponds to a 2-fold non-crystallographic rotation axis. There are few interprotein hydrogen bonding interactions in this homodimer interface, which is composed mainly of non-polar residues (Figure 3). All together, polar and non-polar amino acids contribute a total of 1020 $Å^2$ of buried surface area to the interprotein interface. Four hydrogen bonds are formed across the interface (Figure 3). A large number of non-polar amino acids contribute to this interface with a densely packed core consisting of Trp588, Phe604, Leu602 and Leu596 from one monomer forming Van der Waals interactions with Pro621 and Leu624 from the other monomer. As this interface is found at a 2-fold non-crystallographic axis, the interactions are similar in both half sites. Interestingly, separating both half sites is a water-filled pocket containing the His622 side-chains and with Val624 and Val627 from both monomers forming a water-excluding base so that only one end is solvent accessible. Based on the chromatographic data obtained for the L596R interface-disrupting mutation (below), we demonstrate this is the biochemically relevant salt-dependent tetramer interface.

Gel-filtration chromatography of the XRCC1 and ligase III-α BRCT domains

Previously reported biochemical studies have demonstrated that the X1BRCTb/L3BRCT complex can form tetramers that are favored under lower salt conditions (12). The crystallographic asymmetric unit of the X1BRCTb/L3BRCT structure contains a homodimer of heterodimers. The homodimer interface is formed through the X1BRCTb domains interacting in an identical manner to the homotetramer interface observed in the X1BRCTb homodimer structures (11). However, since this interface is primarily hydrophobic, it was not clear that the association present in the crystal would be favored under

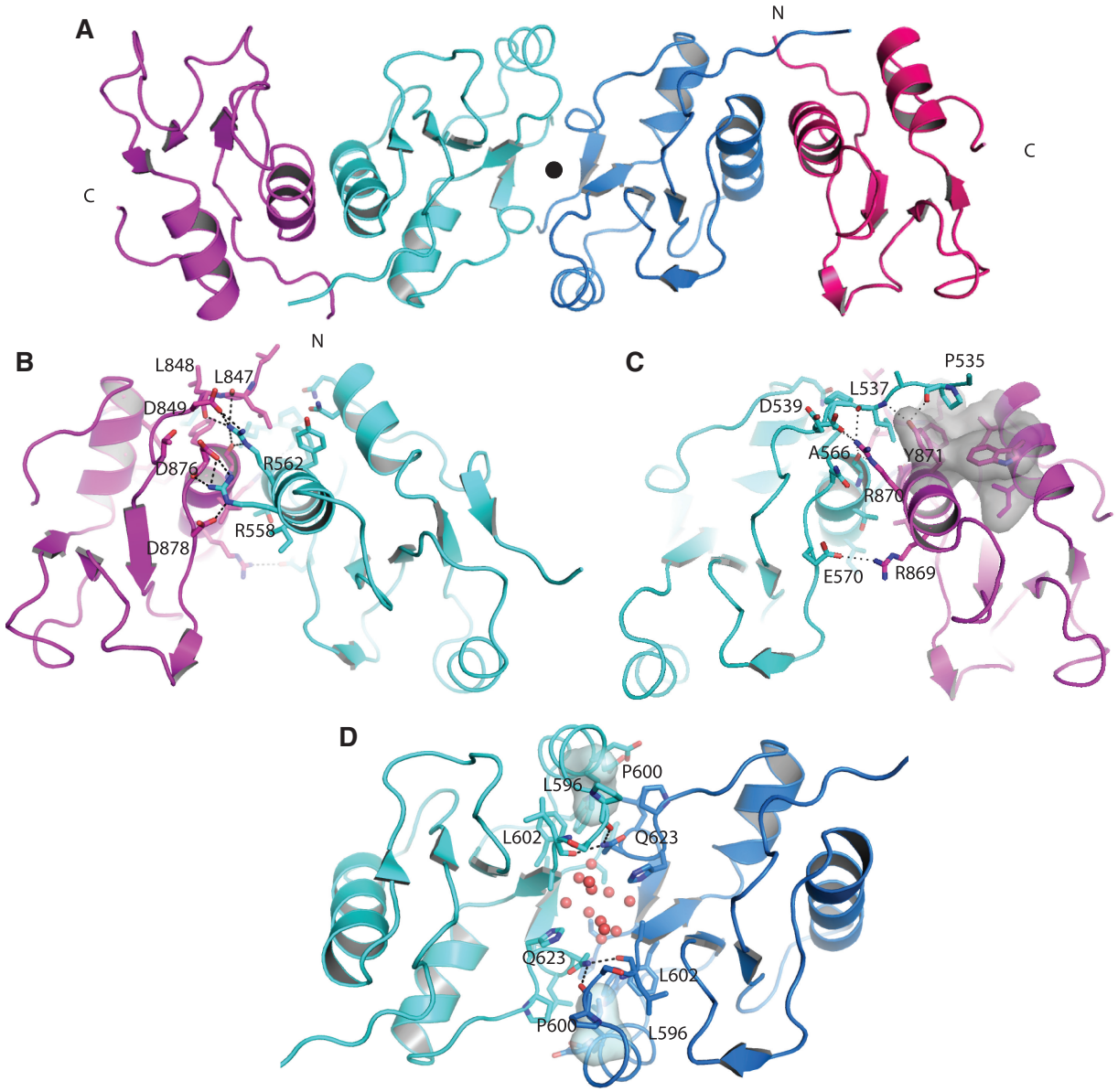

Figure 3. Structure of X1BRCTb/L3BRCT tetramer. (**A**) Overall structure of the tetrameric X1BRCTb/L3BRCT complex (L3BRCT monomers are represented as red and magenta ribbon models; X1BRCTb monomers are represented as blue and cyan ribbon models). The 2-fold non-crystallographic axis in the z-plane of the page is represented as a black circle. (**B**) Close-up view of the X1BRCTb/L3BRCT heterodimer interface (amino acids found at the interface are shown in stick representation. (**C**) X1BRCTb/L3BRCT heterodimer from view (B) rotated 180° about the *y*-axis. The hydrophobic cleft on L3BRCT is shown in a grey surface representation. (**D**) Close-up view of the homodimer interface from the X1BRCTb/L3BRCT heterodimer (amino acids found at the interface are shown in stick representation, L596 is shown as a gray surface and water molecules are shown as red spheres).

lower salt and disrupted under high salt conditions as previously observed.

To determine if the tetramer interfaces are the same in the X1BRCTb homodimer and the X1BRCTb/L3BRCT heterodimer, gel-filtration experiments of these proteins were carried out in the presence of lower, more physiologically relevant (150 mM NaCl) and higher (1 M NaCl) salt conditions (Figure 4). In the presence of 150 mM NaCl, the complex elutes at an apparent molecular mass of 45.0 kDa, whereas under high salt conditions, the complex elutes at an apparent molecular mass of 30.3 kDa; the expected molecular mass is 21.3 kDa. These results are consistent with the behavior previously reported for isolated X1BRCTb (12), suggesting that tetramer formation is mediated through the same X1BRCTb interface. To further evaluate the relevance of this interface, an L596R mutation based on the crystal structure was introduced to disrupt the interface. This mutant elutes from the gel-filtration column in 150 mM NaCl at an apparent molecular weight of 26.2 kDa consistent with disruption of the tetramer interface (Figure 4).

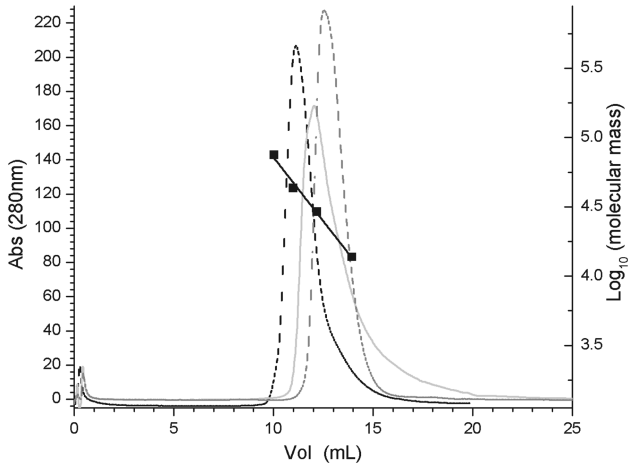

Figure 4. Gel-filtration of X1BRCTb complexed with L3BRCT. X1BRCTb/L3BRCT in 150 mM NaCl (black dashed line) and 1 M NaCl (gray solid line), and X1BRCTb Leu596Arg/L3BRCT in 150 mM NaCl (gray dashed line). The straight line (black) is a fit of the gel filtration standards (black squares) used to estimate the molecular mass of the complexes.

Small-angle X-ray scattering of the mutant heterodimer

The interaction of X1BRCTb with L3BRCT was investigated using small-angle X-ray scattering (SAXS). Both the wild-type proteins and the heterodimer were significantly polydisperse as judged by the SAXS intensity data. However, the observed polydispersity was reduced in samples of a double mutant heterodimeric complex X1BRCTb (Y574R and L596R/wt-L3BRCT). I_o molecular weight analysis of the SAXS data on a 2.0 mg/ml double mutant sample, based upon the scattering of a lysozyme standard, produces the expected molecular weight of 20.7 kDa, consistent with the gel filtration experiments of the single L596R single mutant and the molecular weight based on amino acid composition (21.3 kDa) (Supplementary Table S4). The experimental radius of gyration (19.2 Å) and the intensity scattering profile of the double-mutant heterodimer also match the X-ray crystal structure calculated radius of gyration (19.1 Å) and intensity data (Figure 5 and Supplementary Table S4). The SAXS intensity data was used to construct an *ab initio* model of the mutant heterodimer in solution. The SAXS-based model of this complex has an overall shape consistent with the X-ray crystal structure, indicating that the relative orientation of the monomers seen in the crystal structures is maintained in solution (Figure 5). Additionally, superposition of the SAXS model with the crystal structure model produces an RMSD of 0.92 Å.

Partitioning of L3BRCT homodimers

Many of the hydrogen bonds and hydrophobic interactions contributing to the observed interface are conserved in both proteins. However, additional non-conserved hydrogen bonds found in the X1BRCTb homodimer have interesting implications for heterodimer/homodimer partitioning. Arg558 in X1BRCTb can form a total of six interprotein hydrogen bonds with the side-chains of Glu570 and Asn568, and with the main-chain carbonyl of Gly569. In L3BRCT, the residue corresponding to Arg558 is a serine (Ser866), but the residues corresponding to Glu570 (Asp878), Asn568 (Asp876) and Gly569 (Gly877) are conserved (Figure 6). Indeed, in both L3BRCT homodimers, the analogous hydrogen bonds are missing whereas they are present in the heterodimer. Additionally, Arg869 in the L3BRCT homodimer is also found in an electrostatically unfavorable position relative to Arg869 in the opposite monomer (Figure 6). In the heterodimer, this unfavorable interaction is not present as Arg869 is replaced with an isoleucine in X1BRCTb, so that Arg869 instead hydrogen bonds with the side-chain of Glu570 (Figure 6). In the structure of the ligase homodimer that is characterized by a more closed orientation, these arginine residues adopt an alternate rotamer to alleviate this unfavorable interaction. For the interactions summarized above, the heterodimer allows for the formation of additional hydrogen bonds while alleviating unfavorable electrostatic interactions found in the ligase homodimer. These interactions provide one basis for homodimer/heterodimer discrimination.

Partitioning of X1BRCTb homodimers

Unlike L3BRCT, the X1BRCTb homodimer essentially has the same hydrogen-bonding network as the heterodimer, suggesting homodimer and heterodimer complexes have similar binding constants. We postulated that there must exist mechanisms favoring formation of the heterodimer over the homodimer. Based upon positioning of the N-terminus of the X1BRCTb in the heterodimer, we identified a cluster of surface residues in L3BRCT that appeared to provide a potential binding site for additional N-terminal amino acids that were not present in our crystallization constructs. These N-terminal residues are not conserved in L3BRCT, nor is the analogous cluster of surface residues conserved in X1BRCTb, suggesting a possible role of this groove in partitioning the X1BRCTb homodimer to favor formation of the heterodimer.

To test this hypothesis, a longer chimeric mouse X1BRCTb was constructed that consisted of an additional eight residues from the human XRCC1 on the N-terminus [X1BRCTb(Y574R)-extended]. The heterodimeric structure of X1BRCTb(Y574R)-extended and L3BRCT was solved to a resolution of 2.26 Å. As anticipated, based upon analysis of the original crystal structure, the N-terminus of X1BRCTb(Y574R)-extended formed numerous specific contacts with the ligase (Figure 7). These added N-terminal residues form an additional $\sim 500 Å^2$ of buried surface area for total of 1749 $Å^2$ for the C/D chains of this protein complex. Interestingly, in the A/B chains of this complex, the N-terminus of the ligase is additionally ordered, forming an even larger buried surface area, for a total of 1923 $Å^2$. Both polar and non-polar contacts are made with these extra residues, with Val534 and Pro535A being placed into what would be a solvent exposed hydrophobic pocket in the ligase homodimer. A total of four hydrogen bonds are formed with the additional residues in the extended

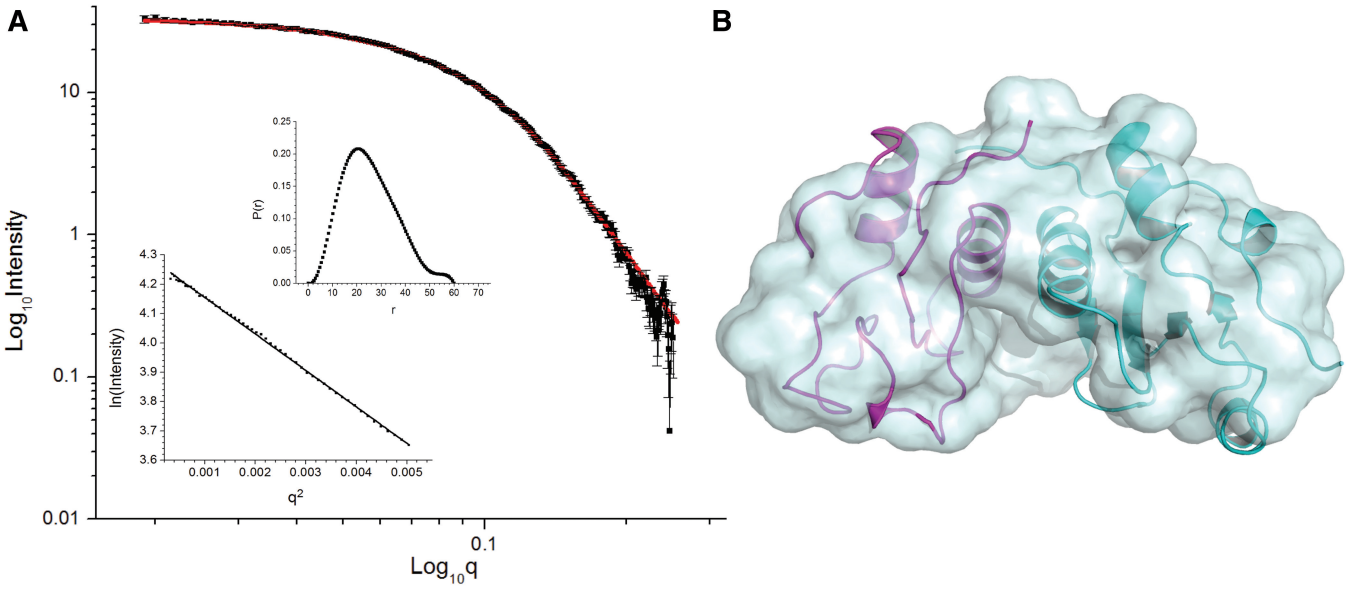

Figure 5. Small-angle X-ray scattering of double mutant heterodimer. (**A**) SAXS intensity data of X1BRCTb(Y574R,L596R)/L3BRCT heterodimer. Black line is the raw scattering data with associated errors and the red line is the fit to the X-ray crystal structure of the X1BRCTb/L3BRCT dimer from the tetrameric crystal structure. Insets are the Guinier fit and the pair-wise distribution function. (**B**) *Ab initio* SAXS envelope model superimposed with the X-ray crystal structure of the X1BRCTb/L3BRCT dimer from the tetrameric crystal structure. X1BRCTb is shown in a cyan ribbon representation and L3BRCT is shown in a magenta ribbon representation.

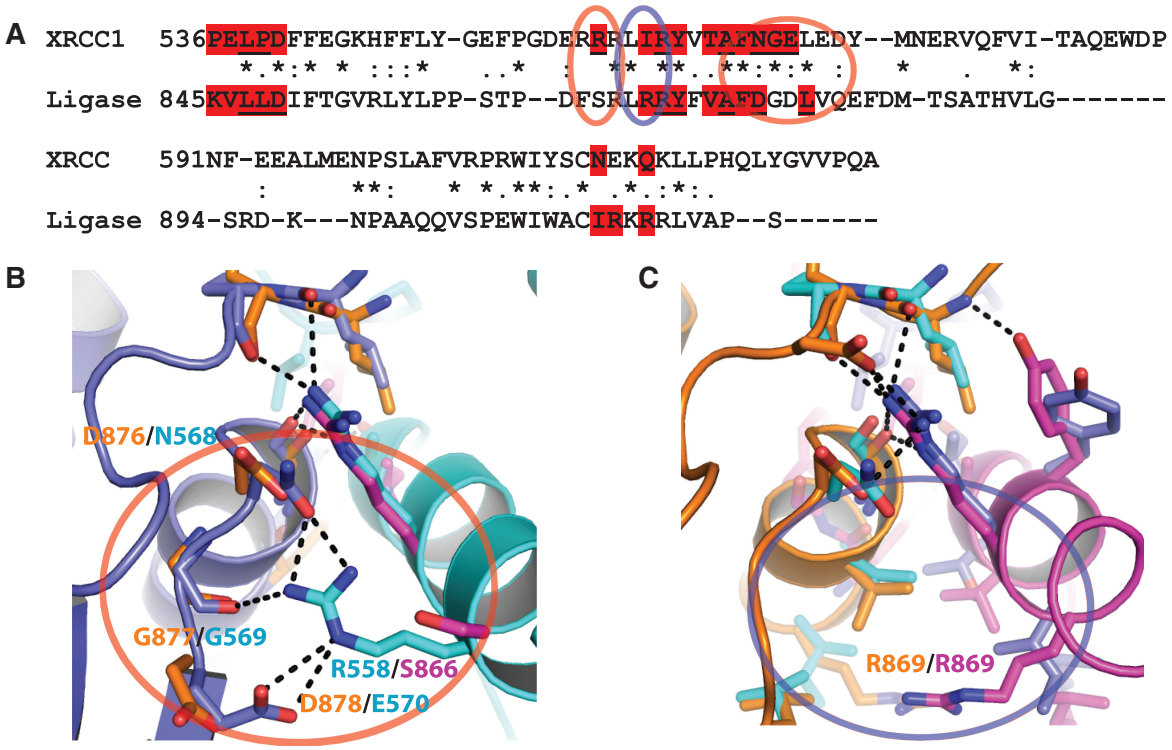

Figure 6. Conservation of X1BRCTb/L3BRCT protein interface residues. (**A**) Amino acid composition of the X1BRCTb and L3BRCT homodimer interface. Amino acids composing the protein interfaces are highlighted in red and those involved in hydrogen-bonding interactions are underlined. (**B**) X1BRCTb hydrogen-bonding network superimposed with the conserved residues from L3BRCT. X1BRCTb monomers are colored in blue tones; side-chains involved in forming the interface and homodimer hydrogen bonds are colored the same, numbered and shown as stick representations. Side-chains from the L3BRCT homodimer are also shown as stick representations that are colored orange and magenta. (**C**) L3BRCT hydrogen bonding network superimposed with the conserved residues from X1BRCTb [colored as in (B)]. Residues circled in (B) and (C) are circled in (A).

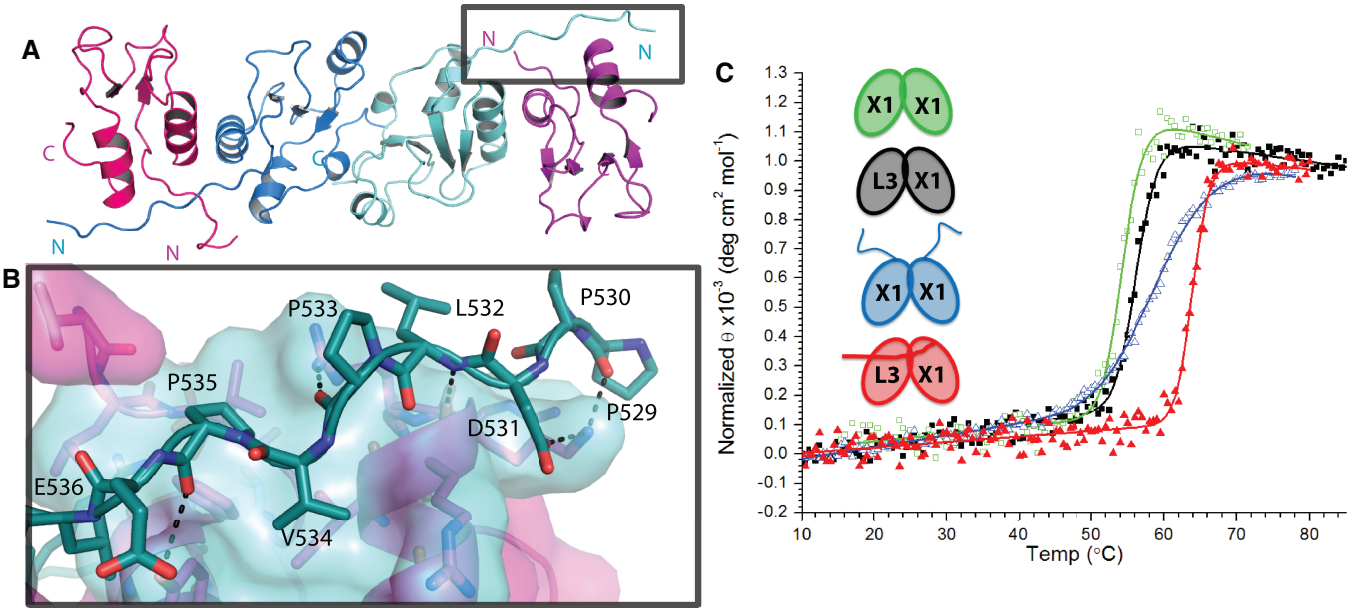

Figure 7. Structure of the X1BRCTb(Y574R)-extended/L3BRCT complex. (**A**) Overall structure of the tetrameric X1BRCTb(Y574R)-extended/L3BRCT complex (L3BRCT monomers are represented as red and magenta ribbon models; X1BRCTb(Y574R)-extended monomers are represented as blue and cyan ribbon models). (**B**) Close-up view of the X1BRCTb-extended/L3BRCT heterodimer interface (amino acids found at the interface are shown in stick representation and amino acids composing the L3BRCT peptide-binding site are shown as a pale green surface; non-interacting surfaces of the ligase are colored in magenta). (**C**) Circular dichroism temperature melts of X1BRCTb (green), X1BRCTb(Y574) extended (blue), X1BRCTb/L3BRCT (black), X1BRCTb(Y574R)-extended/L3BRCT (red). Inset is a schematic representing the constructs used for the temperature melts (X1, X1BRCTb; L3, L3BRCT).

complex, one of which is a salt-bridge between Asp531 of X1BRCTb(Y574R)-extended and Lys915 of the ligase (Figure 7). Two additional amino acids were included in the construct prior to Glu528; however, they were disordered and do not interact with the ligase. The above-mentioned interactions are unlikely to be formed in the X1BRCTb homodimer. The hydrophobic pocket, into which Val534 and Pro535 are placed, is occluded by the side-chain of Asn614 and Gln617 in the X1BRCTb homodimer. Taken together these factors suggest a structural mechanism for a partitioning between homo- and heterodimer complexes.

Thermal melting (T_m) point determinations were performed to further evaluate the stabilizing role of the N-terminus in the heterodimer. The presence of the additional N-terminal residues in the X1BRCTb(Y574R)-extended construct elevated the melting temperature by 7.7 to 63.9°C, compared with the T_m = 56.2°C obtained for the heterodimer lacking the extension (Figure 7).This increase in T_m is directly related to the additional free energy of binding of the extended heteroprotein complex. The T_m of the extended homodimer is 60.3°C, supporting the above-mentioned conclusion that the analogous interactions are not present. There is also a significant decrease in cooperativity of the melting transition, suggesting that these residues in the homodimer lead to destabilization, rather than the stabilization observed in the heterodimer. Additionally, the non-extended X1BRCTb homodimer has a T_m of 54.3°C, only 1.9°C less stable than the shorter heterodimer. This small difference in T_m clearly indicates the shorter heteroprotein complex is only slightly more stable than the X1BRCTb homodimer, and therefore suggests small differences in the binding constants of these complexes, while providing an explanation for the observed crystallization of homodimers from a solution of heterodimer.

DISCUSSION

The continuing identification of binding partners for XRCC1 reflects an evolving understanding of the multiple roles played by this protein in DNA repair processes (1,5,27–29). Coordination of the individual steps involved in DNA repair is of critical importance due to the lability of many of the intermediates involved. XRCC1 is postulated to play a central role in spatial organization of DNA repair factors, facilitating efficient transfer of repair intermediates. Among the many XRCC1 interactions that have been identified, only one, the complex formed with ligase III-α, is considered to be constitutive (1,8,29). This interaction has been shown to stabilize the ligase, increasing the catalytic efficiency of the ligation reaction (6), playing a role in both nucleotide- and base excision repair. The present study contains the first structural characterization of the X1BRCTb/L3BRCT complex that forms the basis for this constitutive interaction, and further demonstrates that a tetramer consisting of two X1BRCTb/L3BRCT heterodimers forms involving direct contact of the two X1BRCTb domains.

The X1BRCTb homodimer was the first BRCT domain to be structurally characterized (11).This structure, in

combination with subsequent modeling studies (13) led to the proposal that BRCT-mediated protein complexes could be based on analogous heterodimers. However, experimental evidence for such structures has proven so elusive that alternative proposals have been advanced, such as the suggestion that the XRCC1/ligase III-α complex involves the association of two BRCT-domain homodimers (12) and the identification of differing binding epitopes of XRCC1 (7,12,30). An additional problem inherent in the heterodimer model results from the lack of an obvious basis for the selection of the heterodimer over the homodimer.

The structures presented here resolve these issues, demonstrating that the X1BRCTb and L3BRCT homodimers as well as the X1BRCTb/L3BRCT heterodimer all utilize a common interface. An alternative ligase-binding element identified by Taylor *et al.* (7) (mouse XRCC1 residues 571–590), which is related to the C1/C3 loop binding epitope discussed by Huyton *et al.* (30), has ~50% amino acid similarity to the heterodimer interface identified here that includes alpha helix 1 and surrounding residues (mouse XRCC1 residues 552–571). This provides a possible explanation for the earlier observation of binding affinity of this construct to L3BRCT. The competitive dimerization dilemma inherent in the earlier proposals has also been resolved with the demonstration that residues in the linker immediately preceding the X1BRCTb domain interact with L3BRCT, significantly expanding the buried surface area and leading to enhanced stability of the heterodimer, as demonstrated by thermal melting curves. Alternatively, analysis of the homodimer structures indicates that no corresponding stabilization would result from analogous interactions in the homodimers. Additionally, based both on the structure reported here as well as the previous NMR study (15), the L3BRCT homodimer complex is less stable than the X1BRCTb homodimer. It is likely that the homodimers serve additional roles, e.g. providing a stable intermediate species in the absence of the heterodimer binding partner that could function to reduce non-specific interactions and/or protein degradation.

BRCT domains are a common protein interaction module serving fundamental roles in cell signaling and DNA repair pathways. The canonical tandem BRCT domain forms an asymmetric homodimer that creates a phosphopeptide binding site (31). The most common BRCT-mediated protein binding modality identified to date involves BRCT repeats with protein domains of different structure. Examples include p53-53BP1 (32,33) and XRCC1/ligase-IV (34). The symmetric heterodimer structure presented here represents an alternative protein-protein dimerization modality. However, all of these BRCT-mediated complexes demonstrate a common strategy of utilizing additional linker residues to achieve greater affinity and specificity.

The interaction of XRCC1 with DNA ligase III-α and the defective DNA repair phenotype associated with its disruption was identified by Caldecott and colleagues (6). Subsequent work demonstrated that the interaction of these proteins was between the C-terminal BRCT domains of each protein, in which the ligase is distally located from the core catalytic domain (7). The question has therefore remained as to why the interaction of XRCC1 with DNA ligase III-α would have an effect on repair efficiency. The structure of the heteroprotein complex provides some insight regarding its function. XRCC1 interacts with both APE1 (2) and DNA polymerase β (35), the enzymes involved in the earlier steps of base excision repair. The interaction of XRCC1 with DNA ligase III-α serves as a means to increase the effective concentration of the ligase at these reaction centers. Moreover, the peptide binding site on the surface of the ligase may be a structural feature involved in positioning the N-terminal domains of XRCC1, and in-turn APE1 and DNA polymerase β, so as to be in an optimal position for hand-off of the DNA repair intermediates to the ligase.

The functional role, if any, of a dimeric repair complex mediated by the observed tetrameric heterodimer interactions remains unknown, however experiments are currently in progress to determine if a defective DNA repair phenotype is associated with the tetramer-disrupting L596R XRCC1 mutation. These experiments may provide insights into the possible role of a dimeric XRCC1 complex in efficient DNA repair.

ACCESSION NUMBERS

3PC6, 3PC7, 3PC8, 3QVG.

SUPPLEMENTARY DATA

Supplementary Data are available at NAR Online.

ACKNOWLEDGEMENTS

The authors would like to thank the Drs Lin Yang and Marc Allaire of the X9 beamline, at the National Synchrotron Light Source at Brookhaven National Laboratory.

FUNDING

Use of the X9 beamline is supported by the US Department of Energy, Office of Science, Office of Basic Energy Sciences, under Contract No. DE-AC02-98CH10886. Data were collected at Southeast Regional Collaborative Access Team (SER-CAT) 22-ID (or 22-BM) beamline at the Advanced Photon Source, Argonne National Laboratory. Use of the Advanced Photon Source was supported by the US Department of Energy, Office of Science, Office of Basic Energy Sciences, under Contract No. W-31-109-Eng-38. Funding for open access charge: The Research Project (Number Z01-ES050111 to R.E.L.); Intramural Research Program of the National Institute of Environmental Health Sciences, National Institutes of Health.

Conflict of interest statement. None declared.

REFERENCES

1. Caldecott,K.W. (2003) XRCC1 and DNA strand break repair. *DNA Repair*, **2**, 955–969.
2. Vidal,A.E., Boiteux,S., Hickson,I.D. and Radicella,J.P. (2001) XRCC1 coordinates the initial and late stages of DNA abasic site repair through protein-protein interactions. *EMBO J.*, **20**, 6530–6539.
3. Masson,M., Niedergang,C., Schreiber,V., Muller,S., Menissier-de Murcia,J. and de Murcia,G. (1998) XRCC1 is specifically associated with poly(ADP-ribose) polymerase and negatively regulates its activity following DNA damage. *Mol. Cell Biol.*, **18**, 3563–3571.
4. Date,H., Igarashi,S., Sano,Y., Takahashi,T., Takano,H., Tsuji,S., Nishizawa,M. and Onodera,O. (2004) The FHA domain of aprataxin interacts with the C-terminal region of XRCC1. *Biochem. Biophys. Res. Commun.*, **325**, 1279–1285.
5. Levy,N., Oehlmann,M., Delalande,F., Nasheuer,H.P., Van Dorsselaer,A., Schreiber,V., de Murcia,G., Menissier-de Murcia,J., Maiorano,D. and Bresson,A. (2009) XRCC1 interacts with the p58 subunit of DNA Pol alpha-primase and may coordinate DNA repair and replication during S phase. *Nucleic Acids Res.*, **37**, 3177–3188.
6. Caldecott,K.W., McKeown,C.K., Tucker,J.D., Ljungquist,S. and Thompson,L.H. (1994) An interaction between the mammalian DNA repair protein XRCC1 and DNA ligase III. *Mol. Cell Biol.*, **14**, 68–76.
7. Taylor,R.M., Wickstead,B., Cronin,S. and Caldecott,K.W. (1998) Role of a BRCT domain in the interaction of DNA ligase III-alpha with the DNA repair protein XRCC1. *Curr. Biol.*, **8**, 877–880.
8. Moser,J., Kool,H., Giakzidis,I., Caldecott,K., Mullenders,L.H. and Fousteri,M.I. (2007) Sealing of chromosomal DNA nicks during nucleotide excision repair requires XRCC1 and DNA ligase III alpha in a cell-cycle-specific manner. *Mol. Cell*, **27**, 311–323.
9. Wang,H.C., Rosidi,B., Perrault,R., Wang,M.L., Zhang,L.H., Windhofer,F. and Iliakis,G. (2005) DNA ligase III as a candidate component of backup pathways of nonhomologous end joining. *Cancer Res.*, **65**, 4020–4030.
10. Thornton,K.H., Krishnan,V.V., West,M.G., Popham,J., Ramirez,M., Thelen,M.P. and Cosman,M. (2001) Expression, purification, and biophysical characterization of the BRCT domain of human DNA ligase IIIalpha. *Protein Expr. Purif.*, **21**, 401–411.
11. Zhang,X., Morera,S., Bates,P.A., Whitehead,P.C., Coffer,A.I., Hainbucher,K., Nash,R.A., Sternberg,M.J., Lindahl,T. and Freemont,P.S. (1998) Structure of an XRCC1 BRCT domain: a new protein-protein interaction module. *EMBO J.*, **17**, 6404–6411.
12. Beernink,P.T., Hwang,M., Ramirez,M., Murphy,M.B., Doyle,S.A. and Thelen,M.P. (2005) Specificity of protein interactions mediated by BRCT domains of the XRCC1 DNA repair protein. *J. Biol. Chem.*, **280**, 30206–30213.
13. Dulic,A., Bates,P.A., Zhang,X., Martin,S.R., Freemont,P.S., Lindahl,T. and Barnes,D.E. (2001) BRCT domain interactions in the heterodimeric DNA repair protein XRCC1-DNA ligase III. *Biochemistry*, **40**, 5906–5913.
14. Ali,M.F., Meza,J.L., Rogan,E.G. and Chakravarti,D. (2008) Prevalence of BER gene polymorphisms in sporadic breast cancer. *Oncol. Rep.*, **19**, 1033–1038.
15. Berquist,B.R., Singh,D.K., Fan,J.S., Kim,D., Gillenwater,E., Kulkarni,A., Bohr,V.A., Ackerman,E.J., Tomkinson,A.E. and Wilson,D.M. (2010) Functional capacity of XRCC1 protein variants identified in DNA repair-deficient Chinese hamster ovary cell lines and the human population. *Nucleic Acids Res.*, **38**, 5023–5035.
16. Konarev,P.V., Volkov,V.V., Sokolova,A.V., Koch,M.H.J. and Svergun,D.I. (2003) PRIMUS: a Windows PC-based system for small-angle scattering data analysis. *J. Appl. Cryst.*, **36**, 1277–1282.
17. Svergun,D.I. (1992) Determination of the regularization parameter in indirect-transform methods using perceptual criteria. *J. Appl. Cryst.*, **25**, 495–503.
18. Svergun,D.I., Petoukhov,M.V. and Koch,M.H. (2001) Determination of domain structure of proteins from X-ray solution scattering. *Biophys. J.*, **80**, 2946–2953.
19. Kozin,M.B. and Svergun,D.I. (2000) Automated matching of high- and low-resolution structural models. *J. Appl. Cryst.*, **34**, 33–41.
20. Schellman,J.A. (1987) The thermodynamic stability of proteins. *Annu. Rev. Biophys. Biophys. Chem.*, **16**, 115–137.
21. Cohen,D.S. and Pielak,G.J. (1994) Stability of yeast iso-1-ferricytochrome c as a function of pH and temperature. *Protein Sci.*, **3**, 1253–1260.
22. Kabsch,W. (1993) Automatic processing of rotation diffraction data from crystals of initially unknown symmetry and cell constants. *J. Appl. Cryst.*, **26**, 795–800.
23. Otwinowski,Z. and Minor,W. (1997) Processing of X-ray diffaction data collected in oscillation mode. *Methods Enzymol.*, **276A**, 307–326.
24. Collaborative Computational Project. (1994) The CCP4 suite: programs for protein crystallography. *Acta Crystallogr. D. Biol. Crystallogr.*, **50**, 760–763.
25. Emsley,P. and Cowtan,K. (2004) Coot: model-building tools for molecular graphics. *Acta Crystallogr. D. Biol. Crystallogr.*, **60**, 2126–2132.
26. Murshudov,G.N., Vagin,A.A. and Dodson,E.J. (1997) Refinement of macromolecular structures by the maximum-likelihood method. *Acta Crystallogr. D. Biol. Crystallogr.*, **53**, 240–255.
27. Clements,P.M., Breslin,C., Deeks,E.D., Byrd,P.J., Ju,L., Bieganowski,P., Brenner,C., Moreira,M.C., Taylor,A.M. and Caldecott,K.W. (2004) The ataxia-oculomotor apraxia 1 gene product has a role distinct from ATM and interacts with the DNA strand break repair proteins XRCC1 and XRCC4. *DNA Repair*, **3**, 1493–1502.
28. Wang,S., Gong,Z., Chen,R., Liu,Y., Li,A., Li,G. and Zhou,J. (2009) JWA regulates XRCC1 and functions as a novel base excision repair protein in oxidative-stress-induced DNA single-strand breaks. *Nucleic Acids Res.*, **37**, 1936–1950.
29. Luo,H., Chan,D.W., Yang,T., Rodriguez,M., Chen,B.P., Leng,M., Mu,J.J., Chen,D., Songyang,Z., Wang,Y. *et al.* (2004) A new XRCC1-containing complex and its role in cellular survival of methyl methanesulfonate treatment. *Mol. Cell Biol.*, **24**, 8356–8365.
30. Huyton,T., Bates,P.A., Zhang,X., Sternberg,M.J. and Freemont,P.S. (2000) The BRCA1 C-terminal domain: structure and function. *Mutat Res.*, **460**, 319–332.
31. Glover,J.N., Williams,-R.S. and Lee,-M.S. (2004) Interactions between BRCT repeats and phosphoproteins: tangled up in two. *Trends Biochem. Sci.*, **29**, 579–585.
32. Derbyshire,D.J., Basu,B.P., Serpell,L.C., Joo,W.S., Date,T., Iwabuchi,K. and Doherty,A.J. (2002) Crystal structure of human 53BP1 BRCT domains bound to p53 tumour suppressor. *EMBO J.*, **21**, 3863–3872.
33. Joo,W.S., Jeffrey,P.D., Cantor,S.B., Finnin,M.S., Livingston,D.M. and Pavletich,N.P. (2002) Structure of the 53BP1 BRCT region bound to p53 and its comparison to the Brca1 BRCT structure. *Genes Dev.*, **16**, 583–593.
34. Wu,P.Y., Frit,P., Meesala,S., Dauvillier,S., Modesti,M., Andres,S.N., Huang,Y., Sekiguchi,J., Calsou,P., Salles,B. *et al.* (2009) Structural and functional interaction between the human DNA repair proteins DNA ligase IV and XRCC4. *Mol. Cell Biol.*, **29**, 3163–3172.
35. Cuneo,M.J. and London,R.E. (2010) Oxidation state of the XRCC1 N-terminal domain regulates DNA polymerase beta binding affinity. *Proc. Natl Acad. Sci. USA*, **107**, 6805–6810.